Mechanism of the Stepwise Dissociation of Fe^{III} Complexes with Tripodal Ligands as Siderophore Models

Guy Serratrice,*[a] Frédéric Biaso,[a] Fabrice Thomas,[a] and Claude Béguin[a]

Keywords: Tripodal ligands / Iron / Kinetics and mechanisms / Dissociation / Catechol / 8-hydroxyquinoline

The acid hydrolysis and formation kinetics of 1:1 ferric complexes with several tripodal hexadentate ligands were investigated over the $[H^+]$ range of 0.02–1.0 M at 25 °C and at an ionic strength of 2.0 M ($NaClO_4/HClO_4$). These ligands are based on a tris(2-aminoethyl)amine (TREN) spacer connected through a tris(amide) moiety to identical pendant bidentate chelating group arms such as catecholate (TRENCAMS, **L^3**), 8-hydroxyquinolinate (O-TRENSOX, **L^0**) or pyridinophenolate (TRENPYPOLS, **L^5**). Mixed ligands with chelating arms such as catecholate and 8-hydroxyquinolinate (TRENSOX2CAMS, **L^1** and TRENSOXCAMS2, **L^2**) were also investigated. An analogue of **L^0** (C-SOX, **L^4**) with a C-pivot scaffold instead of TREN was studied for comparison. The acid hydrolysis reaction was found to proceed in four kinetically distinguishable stages. A common mechanism in the series was followed when the ligand structure was varied. The first stage is very fast and can be attributed to the dissociation of one arm of the tripodal ligand. The second and third stages involve protonation of the complex which induces a change of coordination giving the corresponding tetracoordinated bis(salicylate) complex (coordination with carbonyl and *o*-hydroxy oxygen atoms). The final dissociation of the ligand proceeds in the fourth stage by one or two kinetically detectable steps. For the last step an important structural effect may be observed from 1.2×10^{-5} to 2.2×10^{-2} s^{-1} for the proton-independent step and from 1.2×10^{-6} to 0.18 $M^{-1}s^{-1}$ for the proton-dependent step. Differences in the rates and mechanism between the different tripodal ligands are discussed in terms of the global electrostatic charge of the ligand and the donor ability of the chelating subunit. The C–N bond rotation of the amide moiety and the importance, depending on the charge, of the H-bond network in the partially uncoordinated complexes have also been considered. The role of electrostatics in complex formation is discussed in relation to the Eigen-Wilkins mechanism.

Introduction

Microbial iron bio-availability is largely determined by the coordination chemistry of Fe^{III} with siderophores, a class of organic compounds having a high and specific chelating affinity for this cation.[1−3] Natural (siderophores) or synthetic Fe^{III} chelating agents can be used for therapeutic or agrochemical applications.[4,5] To gain a better understanding of the mechanism of Fe^{III} chelation and transport in biological systems, quantitative evaluations have been reported through measurements of the kinetics of the Fe^{III} uptake and release (through acid hydrolysis) in aqueous solution.[1] A better knowledge of the cleavage of the iron−oxygen bonds in iron chelates can help with the design of new biologically useful ligands, more precisely by improving iron exchange from ligands to proteins. Studying the sensitivity of the iron−oxygen bond to acid hydrolysis is also interesting since it is well known that, in some compartments of the cell (lysozomes for example), lower pH levels are present. There have been extensive kinetic studies of (hydroxamato)Fe^{III} complexes in relation to the predominance of the hydroxamate binding sites in siderophores.[6−13] The most studied, hexadentate desferrioxamine B (DFB, desferal), has three bidentate hydroxamate groups.[8,9] Fe^{III} complexes of dihydroxamate siderophores and siderophore models have been also investigated[7,10,11] but there are a few kinetic data available for the dechelation processes of complexes with other types of ligands.

In particular, numerous ligands having the tripodal structure have been synthesized and the thermodynamic data of their Fe^{III} complexes have been determined. The tripodal structure mimics the backbone of the tris(catecholate) siderophore enterobactin. It is based on tris(2-aminoethyl)amine (TREN) as a spacer. This central organizing unit is connected through a tris(amide) moiety to pendant arms each containing a bidentate chelating group such as catecholate (TRENCAM,[14] TRENCAMS[15]), hydroxamate (TRENDROX[16]), 8-hydroxyquinolinate (O-TRENSOX[17]), pyridinophenolate (TRENPYPOLS[18]) or hydroxypyridonate.[19] These ligands all exhibit strong complexing behavior towards Fe^{III}. Recently, we synthesized mixed tripodal li-

[a] Institut de Chimie Moléculaire de Grenoble, Laboratoire de Chimie Biomimétique, LEDSS, UMR CNRS 5616, Université Joseph Fourier,
B. P. 53, 38041 Grenoble Cedex 9, France
E-mail: guy.serratrice@ujf-grenoble.fr

Supporting information for this article is available on the WWW under http://www.eurjic.org or from the author.

  DOI: 10.1002/ejic.200300396

gands involving both catecholate and hydroxyquinolinate chelating subunits (TRENSOX2CAMS and TRENSOX-CAMS2[20]). They have been shown to be more effective at pH = 7.4 than the parent homopodal ligands TREN-CAMS and O-TRENSOX. Another series of tripodal ligands bearing a C-pivot scaffold with either 8-hydroxyquinoline (C-SOX,[21] COX[22]) or catechol subunits (Cac-CAM[23]) has also been developed in our laboratory. A C-pivot allows the grafting of any desired substituent, e.g. a polyoxyethylene chain, in order to modulate the hydrophile-lipophile balance or the fluorescent group used for labeling.

We previously investigated the dissociation, by acid hydrolysis, of the Fe^{III}-TRENCAMS[15] and Fe^{III}-O-TRENSOX[17b] complexes. Acid hydrolysis has been described by a stepwise mechanism producing the tetracoordinate bis(salicylate) complex and subsequently leading to its complete dissociation. In contrast to the 8-hydroxyquinoline groups, the catecholate groups have been found to be very labile. In this paper, we report an extensive kinetic study on the acid hydrolysis and formation kinetics of 1:1 ferric complexes with the ligands TRENSOX2CAMS (**L^1**), TRENSOX-CAMS2 (**L^2**), CSOX (**L^4**), and TRENPYPOLS (**L^5**). The structures of the ligands together with those of O-TRENSOX (**L^0**) and TRENCAMS (**L^3**) are depicted in Figure 1. The interesting feature of these ligands is the possibility of two modes of coordination for each arm of the ligand depending on the pH: a lowering of the pH leads to a switch from the coordination with the bidentate unit (8-hydroxyquinolinate or catecholate) to the so called salicylate-like mode in which protonation of the pyridine nitrogen atoms or *meta*-phenolic oxygen atoms induce their replacement by the amide carbonyl oxygen atoms (see for 8-hydroxyquinoline as example in Figure 2). Such a switch is proposed for the mechanism of iron release from enterobactin making reduction easier.[24] There are significant structural differences (bidentate subunit, spacer) between these tripodal ligands which therefore make a comparative study particularly interesting in order to elucidate electrostatic and structural factors affecting the dissociation and the formation of complexes. Furthermore, this kinetic investigation provides data necessary to formulate mechanisms by which the complexes are formed and dissociated.

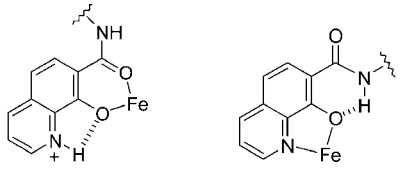

Figure 2. Salicylate (a) and 8-hydroxyquinolinate (b) mode of coordination of **L** with Fe^{III}

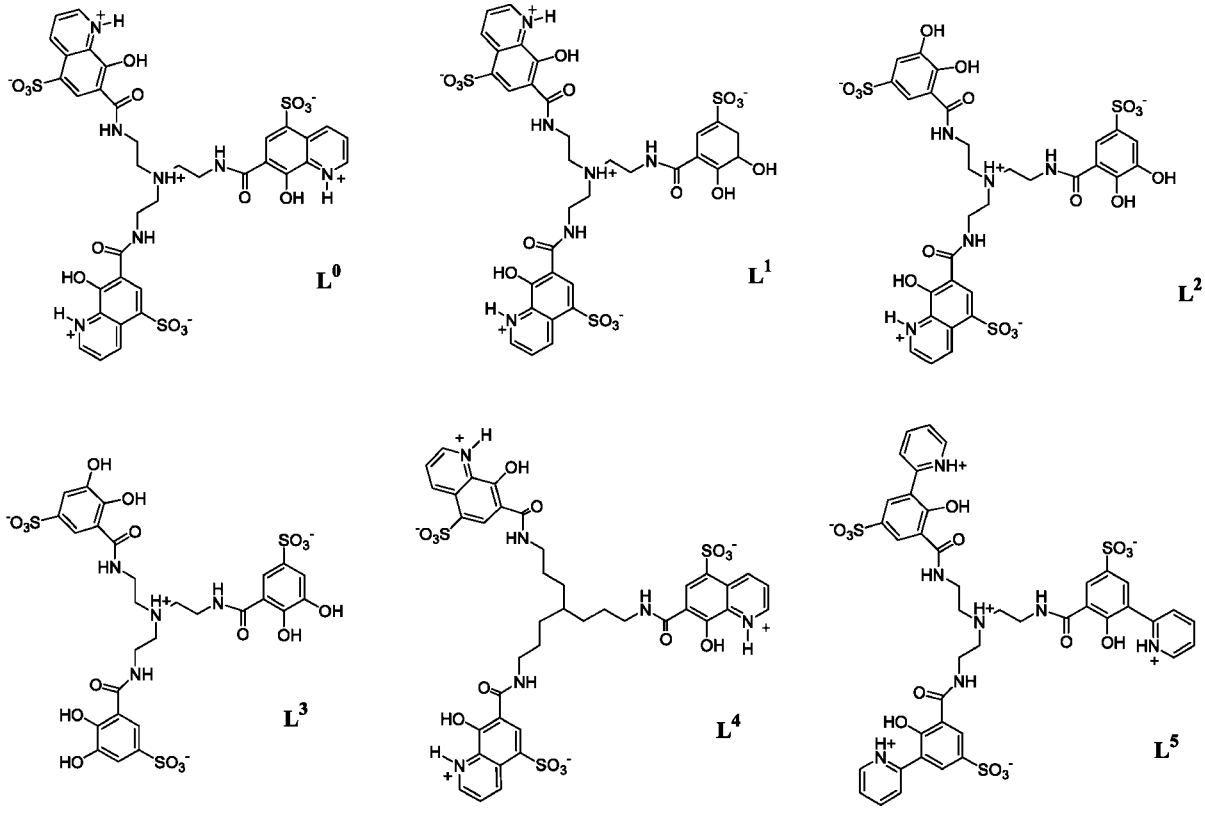

Figure 1. Chemical formulae of the tripodal ligands

Results

Acid Hydrolysis Kinetics

General Observations

All the studied Fe**L**^{n} complexes (n = 0−5 as shown in Figure 1) have been previously characterized by UV/Vis spectrophotometry which showed protonated [Fe**L**^{n}H$_m$] species as the pH was lowered with acidic media.[15,17b,18,20] The acid hydrolysis kinetics of the complexes were investigated in aqueous solution (ionic strength I = 2 M, 25 °C) by the pH jump method under pseudo-first-order conditions with an excess of [H$^+$] (varying generally over the range 0.02−1.0 M) for solutions containing Fe^{III} and the tripodal ligand in a 1:1 molar ratio at an initial pH = 5. The k_{obs} rate constants were determined from the absorbance data versus time at the λ_{max} of the [Fe**L**^{n}] complex. The absorption spectra were also monitored (λ range 300−700 nm) using a diode array device in order to provide additional information on the intermediate species. As the pH was lowered, the spectral changes observed were the result of the change of the number ligands at the iron center and their mode of coordination due to protonation of the coordination sites. The structures of the protonated complexes which were formed during the acid hydrolysis were supported by their absorption spectra.[15,17b,18,20] The acid hydrolysis reaction was found to proceed in three or four kinetically distinguishable stages depending on the ligand. All reaction steps in the first stage were found to occur rapidly and exhibited a loss of absorbance at all the wavelengths (20% of the initial absorbance amplitude for all of the spectrum). This process (denoted stage 1) was too fast to be monitored by stopped-flow measurements and it can been attributed to the dissociation of one arm of the tripodal ligand. The second and the third stages caused a striking change in the spectrum. They involve protonation of the di-coordinated arms which induces a change of coordination to a salicylate mode giving the bis(salicylate) (tetra-coordinated) complex which has been clearly identified from our previous spectrophotometric studies.[15,17b,18,20] Finally, the dissociation of the ligand occurs in the fourth stage in one or two kinetically detectable steps. The successive rate constants are noted k_i where i = 4 and 3 for stages two and three, respectively, i = 2 and 1 for the two steps of the fourth stage (1 is for the last step of the dissociation).

Fe^{III}-TRENSOXCAMS2 (FeL^2)

Four first-order kinetic processes were observed in the [H$^+$] range of 0.001−1 M (Figure 3). The spectrum recorded after the dead time is similar to that of the complex [Fe**L**^{2}H$_3$] with a hydroxyquinolinate and catecholate coordination (λ_{max} = 540 nm) indicating rapid dissociation of a catechol arm and protonation of the tertiary nitrogen atom (Figure , a) since the value of its pK_a = 3.4.[20] A first-order absorbance decay was then measured in the time range of seconds (stage 2). The corresponding pseudo-first-order constant k_4^{obs} was found to vary linearly with [H$^+$] as shown in Figure S1 of the Supporting Information which suggests the rate law (3). The UV/Vis spectra were recorded as a function of the time and the spectrum at the end of stage 2 (Figure 4, b) was found to be similar to the spectrum of the [Fe**L**^{2}H$_4$] species (λ_{max} = 570 nm) having a hydroxyquinolinate coordination and a salicylate coordination with one catecholate arm (through carbonyl and hydroxy oxygen atoms).[20]

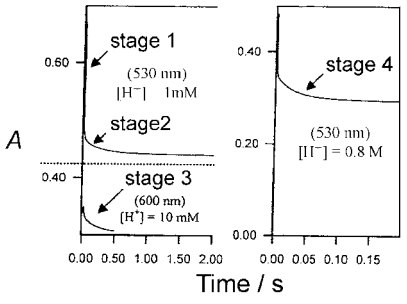

Figure 3. Acid hydrolysis kinetics of the Fe^{III}**L**^{2} complex: absorbance decay at λ = 530 or 600 nm; [Fe^{III}**L**^{2}] = 0.05 mM; [H$^+$] = 1 mM for stages 1 and 2, [H$^+$] = 10 mM for stage 3, [H$^+$] = 0.8 M for stage 4; solvent: water, I = 2 M (NaClO$_4$, HClO$_4$), 25 °C

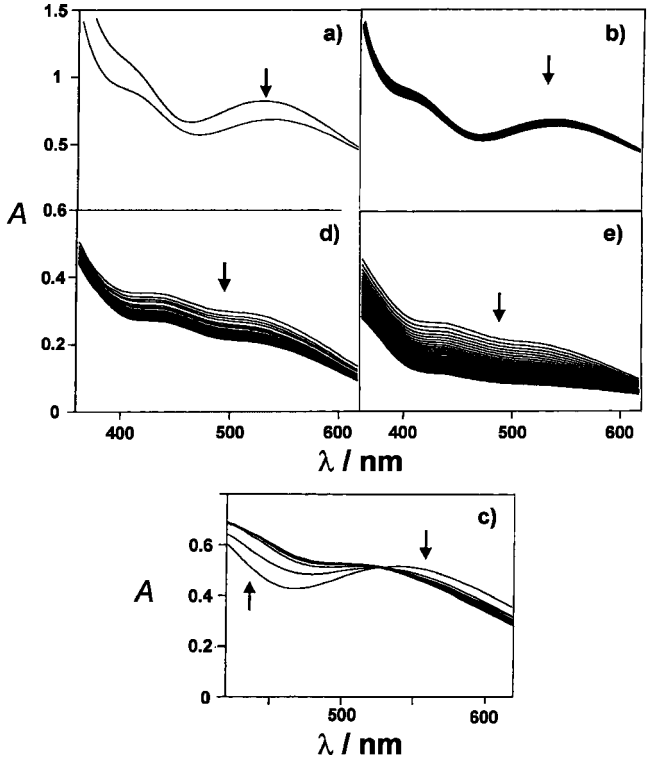

Figure 4. UV/Vis spectra recorded as a function of the time for the acid hydrolysis kinetics of the Fe^{III}**L**^{2} complex: (a) stage 1, 0−3 ms (b) stage 2, 0−1 s (c) stage 3, 0−500 ms (d) stage 4, step 1 0−0.5 s, (e) stage 4, step 2, 0.5−100 s; experimental conditions: see Figure 3; the arrow indicates the direction of change as the reaction proceeds

This is consistent with the following reactions (charges of the complexes and the ligand omitted) from which the

values $k_4 = 4440 \pm 180$ M^{-1} s^{-1} and $k_{-4} \approx 0$ s^{-1} could be deduced [Equations (1)−(3)].

$$Fe\mathbf{L^2} + 3\,H^+ \rightleftarrows Fe\mathbf{L^2}H_3 \text{ (fast)} \quad (1)$$

$$Fe\mathbf{L^2}H_3 + H^+ \rightleftarrows Fe\mathbf{L^2}H_4\ (k_4, k_{-4}) \quad (2)$$

$$k_4^{obs} = k_4\,[H^+] + k_{-4} \quad (3)$$

The third stage exhibited a single-exponential absorbance decay measured at $\lambda = 600$ nm and was monitored over the $[H^+]$ range 0.01−0.07 M. The spectra collected during this stage exhibited an isosbestic point at 525 nm and a decrease of λ_{max} (Figure 4, c) characteristic of the formation of the $Fe\mathbf{L^2}H_5$ species having a bis(salicylate) coordination.[20] The rate constant k_3^{obs} did not show a variation with $[H^+]$ (mean value ≈ 60 s^{-1}, see Figure S2 in the Supporting Information). By analyzing the absorbance data at the end of this stage as a function of $[H^+]^n$ in the form of a Hill plot, a linear plot was obtained for $n = 1$ (Figure S3 in the Supporting Information). These data suggest a saturation behavior with a fast acid-basic pre-equilibrium preceding the rate determining step as given by Equations (4)−(6).

$$Fe\mathbf{L^2}H_4 + H^+ \rightleftarrows Fe\mathbf{L^2}H_5{}^*\ (K_3') \quad (4)$$

$$Fe\mathbf{L^2}H_5{}^* \rightleftarrows Fe\mathbf{L^2}H_5\ (k_3, k_{-3}) \quad (5)$$

$$k_3^{obs} = k_3\,K_3'\,[H^+]/(1 + K_3'\,[H^+]) + k_{-3} \quad (6)$$

Our results imply that $K_3'\,[H^+] >> 1$, so that $k_3^{obs} \approx k_3 + k_{-3}$. Since $[H^+]$ spans the range 0.01−0.07 M, the lower limit for K_3' can be evaluated as ≈10^3 M^{-1}. Since the pK_a value of the equilibrium $Fe\mathbf{L^2}H_5/Fe\mathbf{L^2}H_4$ has been reported as 2.2,[20] it can be inferred that $k_3/k_{-3} < \approx 10^{-0.8}$ ($1/K_a = K_3'k_3/k_{-3}$) allowing evaluation of an upper limit for k_3 as ≈ 10 s^{-1} and k_{-3} as ≈ 50 s^{-1}. The chemical identity of $Fe\mathbf{L^2}H_5{}^*$ will be discussed later.

The spectral change observed during stage 4 showed an absorbance decrease in two steps at all wavelengths (Figure 4, d and e) in two time ranges which is consistent with complete dissociation of the ligand. Two well separated single-exponential absorbance decays (measured at 500 nm) were monitored in the time range of 0.5 s and 100 s over the $[H^+]$ range of 0.2 to 0.65 M. The rate constants k_2^{obs} and k_1^{obs} exhibited linear variations with $[H^+]$ (Figure S4). This result can be interpreted by the successive dissociation reactions. The faster involves dissociation of one arm of the tripodal ligand (charge omitted for $[Fe\mathbf{L^2}H_n]$) [Equations (7) and (8)] with $k_2 = 33.1 \pm 1.9$ M^{-1} s^{-1} and $k_{-2} = 11.2 \pm 1.4$ s^{-1} and the slower involves dissociation of the ligand via two parallel acid-dependent and acid-independent pathways to give free iron(III) in agreement with the dissociation pathways proposed for ferric complexes with the hydroxamate ligand [Equations (9)−(11)[24]][6] {$[FeOH]^{2+}$ for $[Fe(OH)(OH_2)_5]^{2+}$, Fe^{3+} for $[Fe(OH_2)_6]^{3+}$}.

$$Fe\mathbf{L^2}H_5 + H^+ \rightleftarrows Fe\mathbf{L^2}H_6\ (k_2, k_{-2}, K_2) \quad (7)$$

$$k_2^{obs} = k_2\,[H^+] + k_{-2} \quad (8)$$

$$Fe\mathbf{L^2}H_6 + H^+ \rightleftarrows Fe^{3+} + \mathbf{L^2}H_7\ (k_1, k_{-1}, K_1) \quad (9)$$

$$Fe\mathbf{L^2}H_6 + H_2O \rightleftarrows FeOH^{2+} + \mathbf{L^2}H_7\ (k_1', k_{-1}', K_1') \quad (10)$$

$$Fe^{3+} + H_2O \rightleftarrows FeOH^{2+} + H^+\ (K_{Fe} = 0.0015\text{ M}) \quad (11)$$

By assuming relaxation conditions for the reverse reactions, the experimental rate law can be expressed as Equation (12).

$$k_1^{obs} = k_1[H^+] + k_1' + (k_{-1} + k_{-1}'\,K_{Fe}/(K_{Fe} + [H^+])([Fe^{III}]_e + [\mathbf{L^2}H_7]_e) \quad (12)$$

$[Fe^{III}]_e$ and $[\mathbf{L^2}H_7{}^+]_e$ are the total equilibrium concentrations of ligand and metal under our experimental conditions (calculated from absorbances at equilibrium). The term in parentheses calculated using the value of k_{-1}' (2200 M^{-1} s^{-1}) determined from formation kinetics study (vide infra) was found to be negligible (assuming k_{-1} also to be negligible). The fitted values are $k_1 = 0.0137 \pm 0.0005$ M^{-1} s^{-1} and $k_1' = 0.00237 \pm 0.00025$ s^{-1}.

It was found that $K_1\,K_2 = K_1'\,K_2/K_{Fe} = 10^{-2.68}$ is in reasonable agreement with the value $10^{-2.27}$ determined from measurements at equilibrium and at an ionic strength of 0.1 M.[20]

Fe^{III}−TRENSOX2CAMS (FeL^1)

Three distinct first-order kinetic processes could be detected (Figure S5). The spectrum recorded after the dead time suggests a bis-8-hydroxyquinolinate coordination (Figure S6a in the Supporting Information)[20] indicating rapid dissociation of a catechol arm and the formation of the $[Fe\mathbf{L^1}H_3]$ species taking account of the protonation of the tertiary nitrogen. The spectral change observed during stage 2 reflects the change of coordination to a bis(salicylate) mode with the two hydroxyquinoline arms (Figure S6b) in the $[Fe\mathbf{L^1}H_5]$ species. This is clearly supported by its absorbance spectrum.[20] Contrary to the $Fe\mathbf{L^2}$ complex, only one absorbance increase was monitored at 435 nm, in the time range of deciseconds, over the $[H^+]$ range of 0.03 to 0.9 M (Figure S5). It was supposed that formation of the $[Fe\mathbf{L^1}H_4]$ species, corresponding to the change of coordination to a salicylate mode for one 8-hydroxyquinoline arm, was not detectable under our experimental conditions. The absorbance increase allowed determination the rate constant k_3^{obs}. The variation of k_3^{obs} with $[H^+]$ (Figure S7) is linear for $[H^+] > 0.4$ M and exhibits an inverse proton dependence for $[H^+] < 0.4$ M. This behavior can best be

explained by Equations (13)−(15), by analogy with Equations (9)−(11), yielding the rate expression according to Equation (16).

$$Fe\mathbf{L^1}H_4 + H^+ \rightleftarrows Fe\mathbf{L^1}H_5\ (k_3, k_{-3}) \quad (13)$$

$$Fe\mathbf{L^1}H_4 \rightleftarrows Fe\mathbf{L^1}H_4^*\ (k_3', k_{-3}') \quad (14)$$

$$Fe\mathbf{L^1}H_4^* + H^+ \rightleftarrows Fe\mathbf{L^1}H_5\ (K_3'', \text{fast}) \quad (15)$$

$$k_3^{obs} = k_3[H^+] + k_3' + (k_{-3}K_3''[H^+]) + k_{-3}')/(1 + K_3''[H^+]) \quad (16)$$

The non-linear fit of these data give the values $k_3 = 17.9 \pm 1.3$ M^{-1} s^{-1}, $k_{-3}' = 635 \pm 149$ s^{-1}, $K_3'' = 158 \pm 43$ M^{-1} (k_3' and k_{-3} could not be adjusted from the fit). The chemical identity of $Fe\mathbf{L^1}H_4$* and $Fe\mathbf{L^1}H_5$* will be discussed later.

The spectral change observed during stage 3 showed an absorbance decrease at all wavelengths (Figure S6c) and is consistent with dissociation of the ligand from the $Fe\mathbf{L^1}H_5$ species. A mono-exponential absorbance decay (measured at 435 nm) was monitored on a 1000 s time scale over the $[H^+]$ range of 0.2 to 1 M. The variation of k_1^{obs} vs. $[H^+]$ is shown in Figure 5. This can be interpreted by Equations (7) and (9)−(11) (replacing $\mathbf{L^2}$ for $\mathbf{L^1}$) and Equation (12) modified to give Equation (17) by considering Equation (7) as a fast pre-equilibrium.

$$k_1^{obs} = (k_1[H^+] + k_1')K_2[H^+]/(1 + K_2[H^+]) + [k_{-1} + k_{-1}' K_{Fe}/(K_{Fe} + [H^+])]([Fe^{III}]_e + [\mathbf{L^1}H_7]_e) \quad (17)$$

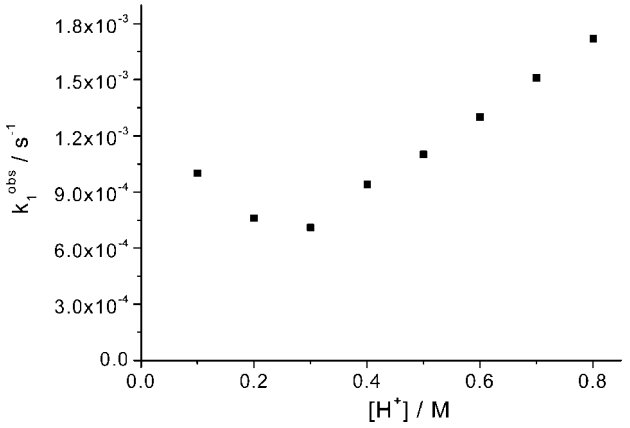

Figure 5. k_1^{obs} [s^{-1}] as a function of $[H^+]$ [M] in the acid hydrolysis kinetics of $Fe\mathbf{L^1}$; $[Fe\mathbf{L^1}] = 0.07$ mM; solvent: water, $I = 2$ M ($NaClO_4$, $HClO_4$), 25 °C

The term in parentheses was calculated using the value of k_{-1}' (1320 M^{-1} s^{-1}) determined from the formation kinetics study (vide infra) and assuming k_{-1} to be negligible. The fitted values are $k_1 = 0.0032 \pm 0.0004$ M^{-1} s^{-1} $k_1' \approx 0$ s^{-1} $K_2 = 1.70 \pm 0.55$ M^{-1}.

It was found that $K_1 K_2 \leq K_1' K_2/K_{Fe} = 10^{-3.55}$ (taking $k_1' \leq k_1/10$) which is in reasonable agreement with the value of $10^{-3.21}$ determined from measurements at equilibrium.[20]

Fe^{III}−CSOX (FeL^4)

Four distinct stages could be detected by measuring the absorbance decay at 600 nm (Figures S8 and S9). After the dead time, a bi-exponential decay of the absorbance was observed on a 10 s time scale with $[H^+]$ in the range of 0.02−0.1 M (stages 2 and 3). This decay could be fitted with a sum of two exponentials [Equation (18)].

$$A = A + A_1\exp(-k_4^{obs}\, t) + A_2\exp(-k_3^{obs}\, t) \quad (18)$$

The rate constants k_4^{obs} and k_3^{obs} vary apparently with $[H^+]$ with a non-zero intercept (Figure S10). This suggests two reversible elementary steps [Equations (19) and (20)].

$$Fe\mathbf{L^4}H_2 + H^+ \rightleftarrows Fe\mathbf{L^4}H_3\ (k_4, k_{-4}) \quad (19)$$

$$Fe\mathbf{L^4}H_3 + H^+ \rightleftarrows Fe\mathbf{L^4}H_4\ (k_3, k_{-3}) \quad (20)$$

The matrix formulation of the rate equations allows determination of analytical expressions for the observed rate constants. The following expressions can thus be deduced [Equations (21) and (22).

$$k_4^{obs} + k_3^{obs} = (k_4 + k_3)[H^+] + k_{-4} + k_{-3} \quad (21)$$

$$(k_4^{obs} - k_3^{obs})^2 = (k_4[H^+] + k_{-4})^2 + (k_3[H^+] + k_{-3})^2 + 2k_{-4}(k_3[H^+] - k_{-3}) - 2k_4(k_3[H^+] + k_{-3}) \quad (22)$$

The four microscopic constants were extracted from a non-linear least-squares refinement of the data according to Equations (21) and (22): $k_4 = 189 \pm 9$ M^{-1} s^{-1}, $k_{-4} = 10.0 \pm 0.4$ s^{-1}, $k_3 = 18.1 \pm 0.9$ M^{-1} s^{-1}, $k_{-3} = 1.20 \pm 0.05$ s^{-1}.

The spectral change observed during stage 4 showed an absorbance decrease at all wavelengths (Figure S9) and is consistent with dissociation of the ligand. A mono-ex-

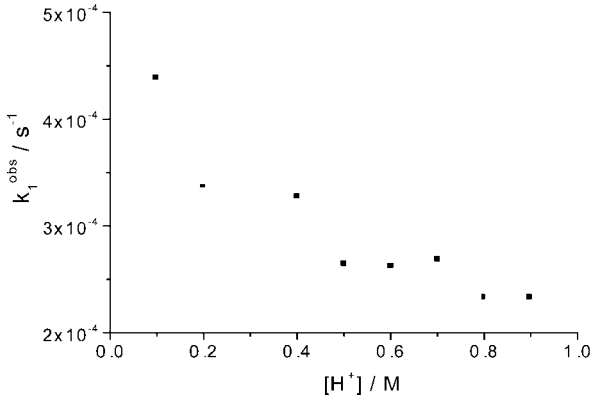

Figure 6. k_1^{obs} [s^{-1}] as a function of $[H^+]$ [M] in the acid hydrolysis kinetics of $Fe\mathbf{L^4}$; $[Fe\mathbf{L^4}] = 0.1$ mM; solvent: water, $I = 2$ M ($NaClO_4$, $HClO_4$), 25 °C

ponential absorbance decay (measured at 435 nm) was monitored on a 10000 s time scale over the $[H^+]$ range of 0.1−1 M. The variation of k_1^{obs} vs. $[H^+]$ is shown in Figure 6.

This can be interpreted by Equations (9)−(11) and Equation (12) (by replacing FeL^2H_5 for FeL^1H_6 and L^2H_7 for L^1H_6). The term in parentheses was calculated using the value of k_{-1}' (1750 M^{-1} s^{-1}) determined from the formation kinetics study (vide infra) and assuming k_{-1} to be negligible. The fitted values are: $k_1' = (2.0 \pm 0.2) \times 10^{-4}$ s^{-1} and $k_1 \approx 0$ M^{-1} s^{-1}.

Fe^{III}−O−TRENSOX (FeL^0)

The acid hydrolysis kinetics have been previously published.[17b] Only the last step of the dissociation was not described. As for **Fe^{III}−CSOX**, release of the ligand is very slow (20000 s time scale) even at high H^+ concentrations. It was observed at 435 nm as a mono-exponential absorbance decay. The variation of k_1^{obs} vs. $[H^+]$ is shown in Figure 7. The fitted values from Equation (13) are $k_1' = 1.0 \times 10^{-5} \pm 1.0 \times 10^{-6}$ s^{-1} and $k_1 \approx 0$ M^{-1} s^{-1} [the term in parentheses in Equation (12) was calculated using the value of 789 M^{-1} s^{-1} for k_{-1}' [17b] and assuming k_{-1} to be negligible].

Fe^{III}−TRENPYPOLS (FeL^5)

The absorbance change was measured at 470 nm. Three stages were observed in the $[H^+]$ range of 0.001−1 M (Figure S11). The spectrum change after the dead time resulted in a decrease of λ_{max} from 495 to 469 nm (Figure S12a) and was attributed to the formation of a tetra-coordinated complex with one arm of the tripodal ligand in the pyridinophenolate coordination mode and the other in the salicylate coordination mode.[18] This very fast process was followed by a slight increase in the absorbance at 470 nm (stage 2) in the time range of 200 ms. The UV/Vis spectra recorded as a function of the time (Figure S12b) exhibited an isosbestic point at 540 nm and the spectrum at the end of this stage is similar to that of the bis(salicylate) complex $[FeL^5H_5]$.[18] The corresponding pseudo first-order constant k_3^{obs} was found to vary linearly with $[H^+]$ (Figure S13).

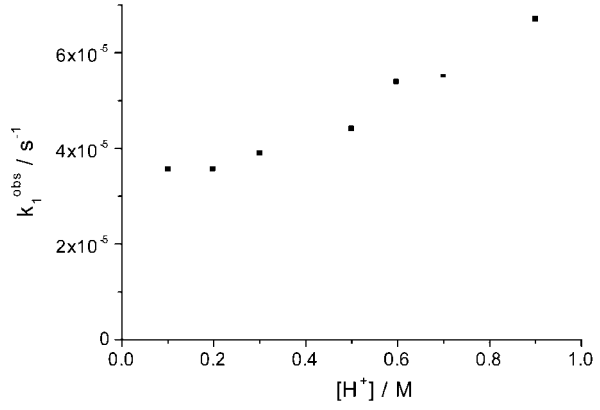

Figure 7. k_1^{obs} $[s^{-1}]$ as a function of $[H^+]$ [M] in the acid hydrolysis kinetics of FeL^0; $[FeL^0]$ = 0.07 mM; solvent: water, I = 2 M ($NaClO_4$, $HClO_4$), 25 °C

This is consistent with the reaction according to Equation (23) and and the rate law according to Equation (24) yielding the values $k_3 = 36 \pm 3$ M^{-1} s^{-1} and $k_{-3} = 18 \pm 1$ s^{-1}, respectively.

$$FeL^5H_4 + H^+ \rightleftarrows FeL^5H_5 \; (k_3, k_{-3}, K_3) \quad (23)$$

$$k_3^{obs} = k_3 [H^+] + k_{-3} \quad (24)$$

The spectral change observed during stage 3 showed an absorbance decrease at all wavelengths (Figures S12c and S12d) and resembles the spectra recorded for the formation reaction study. This is consistent with complete dissociation of the ligand. Two well-separated single-exponential absorbance decays (measured at 470 nm) were monitored in the time range of 5 s and 100 s over the $[H^+]$ range of 0.1−1 M. The rate constants k_2^{obs} exhibited linear variations with $[H^+]$ (Figure S14). The rate constants k_1^{obs} exhibited a linear proton dependence for $[H^+] > 0.2$ M and an inverse proton dependence for $[H^+] < 0.1$ (Figure 8). These successive dissociation reactions are consistent with reactions and rate laws according to Equations (7)−(12) (by replacing FeL^2H_5 with FeL^5H_5 and L^2H_7 with L^5H_7). The rate constants for Equation (7) have been determined as $k_2 = 4.9 \pm 0.2$ M^{-1} s^{-1}; $k_{-2} = 2.1 \pm 0.1$ s^{-1} and for Equations (9) and (10) the following could be evaluated from a non-linear least-squares fit of Equation (11) by taking for k_{-1}' the value of 514 M^{-1} s^{-1} determined from the formation kinetic studies (vide infra) and assuming k_{-1} to be negligible: $k_1 = (7.9 \pm 1.0) \times 10^{-3}$ M^{-1} s^{-1}; $k_1' = (9.6 \pm 5.7) \times 10^{-4}$ s^{-1}.

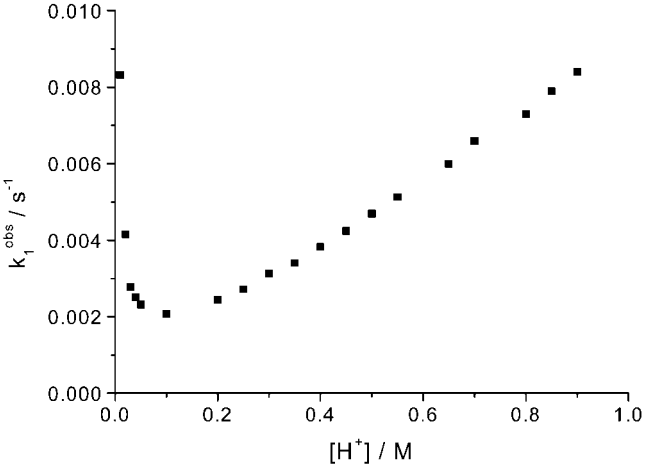

Figure 8. k_1^{obs} $[s^{-1}]$ as a function of $[H^+]$ [M] in the acid hydrolysis kinetics of FeL^5; $[FeL^5]$ = 0.2 mM; solvent: water, I = 2 M ($NaClO_4$, $HClO_4$), 25 °C

It was found that $K_1 K_2 = K_1' K_2 / K_{Fe} = 10^{-2.54}$ which is in reasonable agreement with the value of $10^{-1.79}$ determined from measurements at equilibrium.[18] The values of k_1, k_1', k_2, and k_{-2} for all the complexes are collected in Table 1.

Table 1. Microscopic rate constants for the dissociation of the Fe$\mathbf{L}^{n}H_5$ (except for $\mathbf{L^4}$, Fe$\mathbf{L^4}H_4$) complexes

k_i [M^{-1} s^{-1}] (k_{-i} [s^{-1}])	Fe$\mathbf{L^0}$	Fe$\mathbf{L^1}$	Fe$\mathbf{L^2}$ [a]	Fe$\mathbf{L^3}$ [b]	Fe$\mathbf{L^4}$	Fe$\mathbf{L^5}$
k_2 (k_{-2})	–	–	33.1 (11.2)	fast	–	4.9 (2.1)
$10^3 \times k_1$	< 0.0012	3.2	13.7	184	< 0.02	7.9
$10^3 \times k'_1$ [s^{-1}]	0.012	< 0.32	2.37	22	0.20	0.96
$10^{-3} \times k'_{-1}$ [M^{-1} s^{-1}]	0.789	1.32	2.24	2.7	1.75	0.51

[a] Ref.[17b] [b] Ref.[15]

Formation Kinetics

The kinetics of formation of the ferric complex with ligands $\mathbf{L^1}$, $\mathbf{L^2}$, $\mathbf{L^4}$ and $\mathbf{L^5}$ were investigated by a stopped-flow spectrophotometric method under pseudo-first-order conditions: [Fe^{III}] and [H$^+$] >> [$\mathbf{L}^n$] and at an ionic strength I = 2 M at 25 °C. The absorbance change vs. time at λ = 435 nm showed a single exponential curve indicating that the complex formation reaction proceeds through a single rate-limiting step. It should be noted that the spectra recorded with time using a diode array device were identical to those recorded for the final step of acid hydrolysis. It has been found that the pseudo-first-order rate constants k^{obs} at a given acidity level ([H$^+$] varied from 0.03 to 1 M) show a linear variation as a function of [Fe^{III}]$_{tot}$ with a zero intercept, and at a given concentration of Fe^{III} have a linear variation as a function of 1/[H$^+$] (Figure 9, a as an example). This suggests that the main reaction is the formation of the complex [Fe$\mathbf{L}^{n}H_6$] through the hydrolyzed ferric ion FeOH^{2+} {for [Fe(OH)(OH$_2$)$_5$]$^{2+}$} according to Equation (10) (formation is the reverse reaction). This leads to the observed pseudo-first-order rate constant given by Equation (25), where [Fe^{3+}] = [Fe^{3+}]$_{tot}$ – [FeOH]$^{2+}$ – 2 [Fe$_2$(OH)$_2$]$^{4+}$ and [H$^+$] takes into account the protons involved in formation of FeOH^{2+} [Equation (11)] and the dimer Fe$_2$(OH)$_2^{4+}$ {for [Fe$_2$(OH)$_2$(OH$_2$)$_8$]$^{4+}$} [Equation (26)].[25]

$$k_{obs} = k_{-1}' K_{Fe} [Fe^{3+}]/[H^+] + k_1' \quad (25)$$

$$2\ Fe^{3+} \rightleftarrows Fe_2(OH)_2^{4+} + 2\ H^+ \ (K_{DFe} = 0.0024\ M) \quad (26)$$

A linear variation of k_{obs} versus [Fe^{3+}]/[H$^+$] was observed (Figure 9, b for $\mathbf{L^1}$, Figure S15 for $\mathbf{L^2}$, Figure S16 for $\mathbf{L^4}$ and Figure S17 for $\mathbf{L^5}$). Least-squares fits of the data yielded the values of k_{-1}' 1320 ± 60, 2240 ± 120, 1750 ± 40 and 514 ± 8 M^{-1} s^{-1} for $\mathbf{L^1}$, $\mathbf{L^2}$, $\mathbf{L^4}$ and $\mathbf{L^5}$, respectively ($k_1' \approx 0$ s^{-1} for all cases). The values of k_{-1}' are collected in Table 1 together with the values previously determined for the formation of Fe$\mathbf{L^0}$ and Fe$\mathbf{L^3}$.

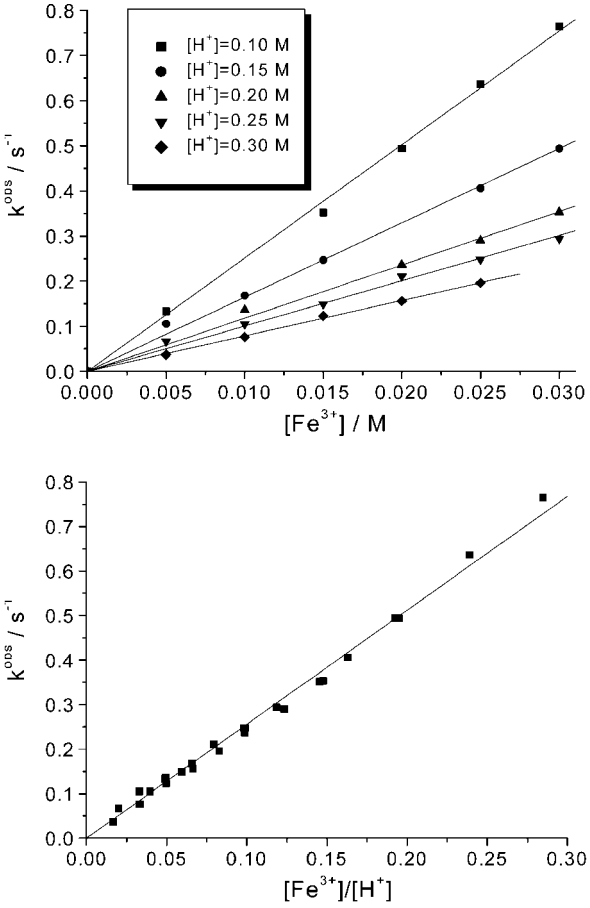

Figure 9. Complex formation kinetics of $\mathbf{L^1}$ with Fe^{III}: (a) k_{obs} [s^{-1}] as a function of [Fe^{3+}]$_{tot}$ [M] at various [H$^+$] [M]; [$\mathbf{L^1}$] = 0.1 mM; (b) k_{obs} [s^{-1}] as a function of [Fe^{3+}]/[H$^+$] according to Equation (25); solvent: water, I = 2 M (NaClO$_4$, HClO$_4$), 25 °C

Discussion

Dissociation Kinetics

Rate constant data for the stepwise acid dissociation of the Fe$^{III}\mathbf{L}^{n}$ complexes are summarized in Tables 1 and 2, including data already published for O–TRENSOX[17b] ($\mathbf{L^0}$) and O–TRENCAMS[15] ($\mathbf{L^3}$). For easy comparison of the kinetic data of stages 1–3, we have reported in Table 2 the state of protonation of the tertiary nitrogen atom (for $\mathbf{L^0}$, $\mathbf{L^1}$, $\mathbf{L^2}$, $\mathbf{L^3}$ and $\mathbf{L^5}$) and the mode of coordination of Fe^{III} in the different species according to the state of protonation, the number of arms coordinated to the metallic cation and the bidentate coordination (8-hydroxyquinolinate or -catecholate or -salicylate). The following discussion suggests elementary reaction pathways as depicted in Figure 10 for Fe$\mathbf{L^2}$, Figure S18 for Fe$\mathbf{L^1}$ and Figure 14 of ref.[17b] for Fe$\mathbf{L^0}$, as examples.

Table 2. Recapitulative table of the measured hydrolysis rate constants for Fe**L″** → Fe**L″**H_5 including modes of protonation and coordination for each stage (charges are omitted)

Ligand	Species[a]	k_n [$M^{-1}s^{-1}$]	k_{-n} [s^{-1}]	Tertiary N[b]	Mode of coordination[c]
L^0	Fe**L^0**H			NH	NO/NO/NO
Ref.[17b]		fast			
	Fe**L^0**H_3			NH	NO/NO/free
	k_4	643	15		
	Fe**L^0**H_4			NH	NO/OOsal(ox)/free
	k_3	5.7	1.3		
	Fe**L^0**H_5			NH	OOsal(ox)/OOsal(ox)/free
L^1	Fe**L^1**			N	NO/NO/OO
		fast			
	Fe**L^1**H_2			N	NO/NO/free
	Fast	−			
	Fe**L^1**H_3			NH	NO/NO/free
	k_4	−	−		
	Fe**L^1**H_4			NH	NO/OOsal(ox)/free
	k_3	17.9			
	Fe**L^1**H_5			NH	OOsal(ox)/OOsal(ox)/free
	$K_3'' = 158$	−			
	Fe**L^1**H_4*			N	OOsal(ox)/OOsal(ox)/free
L^2	Fe**L^2**H			NH	NO/OO/OO
	Fe**L^2**H_3			NH	NO/OO/free
	k_4	4440	< 1		
	Fe**L^2**H_4			NH	NO/OOsal(cat)/free
	$K'_3 > 1000$	fast			
	Fe**L^2**H_5*			NH	O(ox)/OOsal(cat)/free
	k_3	< 10 s^{-1}	ca. 50		
	Fe**L^2**H_5			NH	OOsal(ox)/OOsal(cat)/free
L^3	Fe**L^3**H			NH	OO/OO/OO
Ref.[15]		fast			
	Fe**L^3**H_3			NH	OO/OO/free
		fast			
	Fe**L^3**H_5			NH	OOsal(cat)/OOsal(cat)/free
L^4	Fe**L^4**			C	NO/NO/NO
		fast			
	Fe**L^4**H_2			C	NO/NO/free
	k_4	189	10.0		
	Fe**L^4**H_3			C	NO/OOsal(ox)/free
	k_3	18.1	1.2		
	Fe**L^4**H_4			C	OOsal(ox)/OOsal(ox)/free
L^5	Fe**L^5**H			NH	NO*/NO*/NO*
		fast	−		
	Fe**L^5**H_3			NH	NO*/NO*/free
	k_4	fast	−		
	Fe**L^5**H_4			NH	NO*/OO*sal/free
	k_3	36	18		
	Fe**L^5**H_5			NH	OO*sal/OO*sal/free

[a] The different states of protonation during the pH jump (see text). [b] State of protonation of the anchor. [c] The coordination atoms of the three arms, separated by /, in the reverse order of the complete removal of the *n*th arm with Fe^{III}: "free" indicates an arm without a coordination bond to the iron atom, NO (NO*) refers to 8-hydroxyquinolinate (pyridinophenolate) bidentate coordination to Fe^{III}, OO refers to catecholate bidentate coordination to Fe^{III}, OOsal(ox) indicates salicylate bidentate coordination of a hydroxyquinoline arm to Fe^{III}, OOsal(cat) refers to salicylate bidentate coordination of a catechol arm to Fe^{III}, OO*sal represents salicylate bidentate coordination of a pyridinophenol arm to Fe^{III}.

Stage 1

On the basis of the spectral change, the reaction steps in this stage have been attributed to the dissociation of one arm of the ligand. This process is very fast whatever the type of chelating group. This suggests that the steric strain release in the complex may increase the rate of Fe−O and (or) Fe−N_{pyr} cleavage. We can also invoke, for the high kinetic lability of the hexacoordinate complex, the solvent rearrangement resulting from dissociation of the first bidentate group, as already supported for hydroxamate dissociation.[6] It can be suggested that the dissociated arm is maintained in proximity to the first coordination sphere of Fe^{III} through hydrogen bonds between the water molecules coordinated to Fe^{III} and the free arm. This results in a small motion of the arm as it dissociates from the Fe^{III} center

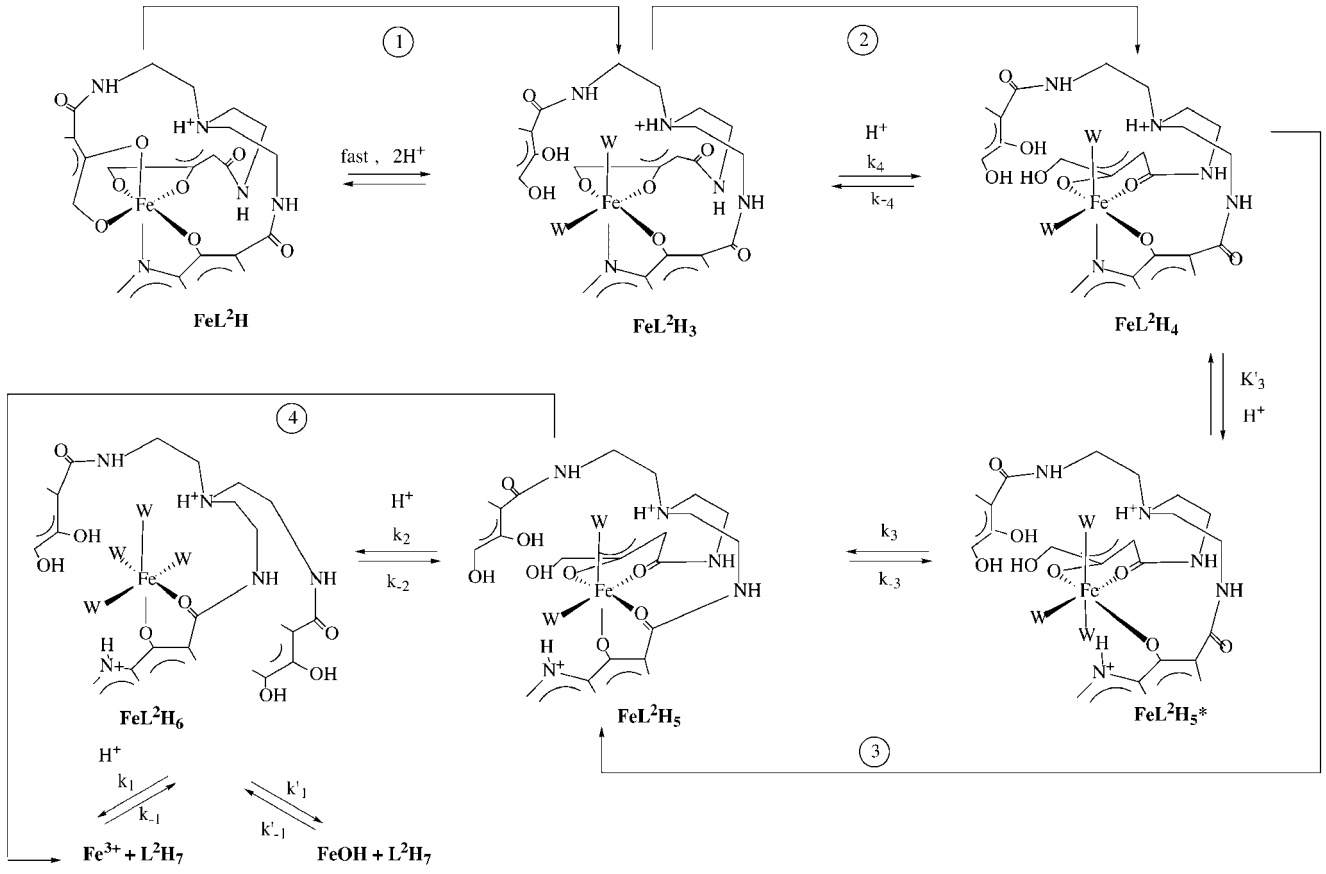

Figure 10. Proposed mechanism for the acid hydrolysis of the Fe$\mathbf{L^2}$H complex

and a slight solvent rearrangement. The reaction from the hexadentate to the tetradentate complex may therefore be a facile process.

Stages 2 and 3

Overall Scheme

These stages result in the formation of a bis(salicylate)-coordinated complex Fe$\mathbf{L}^n$H$_5$ (except Fe$\mathbf{L^4}$H$_4$) as clearly indicated by the spectra recorded at the end of stage 3 in agreement with the equilibrium studies previously published. Each stage is related to one arm of the ligand. It may involve the Fe−N$_{pyr}$ or Fe−O (depending on the type of bidentate group in $\mathbf{L}^n$) bond cleavage with protonation of N or O leading to an open-ring structure with the bidentate moiety, followed by the Fe−O(=C) bond closing the salicylate ring. It should be noted that this change of coordination requires conformational reorganization of the arm by rotation about the C−N amide bond in order to allow the carbonyl group to be in a suitable position favorable for salicylate coordination. Indeed, it has been shown that the carbonyl group is turned outside the Fe^{III} coordination sphere owing to hydrogen bond between the amide hydrogen atom and the *ortho*-oxygen atom (quinolinol or catechol or phenol) when Fe^{III} is coordinated with the bidentate group of each arm, as clearly evidenced.[22,26] We were able to obtain information on several elementary steps corresponding to stages 2 and 3 and rate constants k_4 and k_3, depending on the structure of the tripodal ligand, homopodand or heteropodand, and on the nature of the chelating subunit (catecholate, 8-hydroxyquinolinate, pyridinophenolate). Interesting correlations of the rate constants for same type of process with the chemical structures can be made.

Stages 2 and 3 for the Homopodate Fe$\mathbf{L}^n$H$_3$ Complexes (n = 0, 3, 4, 5)

The values of k_4 and k_3 clearly indicate the more labile character of the catechol arms (fast for the two arms in Fe$\mathbf{L^3}$H$_3$) compared with the pyridinophenol arms (first arm: fast, second arm: 36 M^{-1} s^{-1} in Fe$\mathbf{L^5}$H$_3$) and the 8-hydroxyquinoline arms (first arm: 643 and 189 M^{-1} s^{-1}, second arm: 5.7 M^{-1} s^{-1} and 18.1 M^{-1} s^{-1} in Fe$\mathbf{L^0}$H$_3$ and Fe$\mathbf{L^4}$H$_2$, respectively). This reflects (i) the higher donor strength of catecholate vs. pyridinophenolate and 8-hydroxyquinolinate which increases the electron density of the metal so that the bonds with the coordinated donor atoms are weakened; (ii) the chelate bulkiness which influences the rate of rotation about the C−N amide bond (pyridinophenol vs. catechol); (iii) the easier rotation of the am-

ide bond in the catechol arm compared with in the 8-hydroxyquinoline arm that can be related to the electron-withdrawing effect of the 8-hydroxyquinoline group as clearly shown from the pK_a values of the carboxylic groups in the 2,3-dihydroxybenzoic acid (2.7) and in the 7-carboxy-8-hydroxyquinoline (1.9).[27]

Stages 2 and 3 for the Heteropodate FeL^nH_3 Complexes (n = 1, 2)

The reaction scheme developed from the analysis of the kinetic data is slightly different than for the homopodate complexes. For $\mathbf{L^1}$, only the stage $Fe\mathbf{L^1}H_4/Fe\mathbf{L^1}H_5$ was detected and can be described by Equations (13)−(15). This scheme, developed from an analysis of the kinetic data, has been proposed since the pK_a values of the tertiary amine nitrogen atom (1.9) and of the two hydroxyquinoline nitrogen atoms (2.4) are close.[20] We assumed a complicated kinetic pattern involving an acid-basic micro-equilibrium. A pictorial view of the proposed scheme is shown in Figure S18 (see also Table 2 for the state of protonation). The equilibrium between $Fe\mathbf{L^1}H_4$ and $Fe\mathbf{L^1}H_4$* [Equation (14)] involves proton transfer between the tertiary nitrogen atom and the quinoline nitrogen atom coordinated to the iron center, leading to the change of coordination of the 8-hydroxyquinoline moiety. The reaction according to Equation (15) involves the protonation of the tertiary amine nitrogen atom. The k_3 value (17.9 M^{-1} s^{-1}) is similar to the corresponding values determined for $Fe\mathbf{L^0}H_4$ (5.7 M^{-1} s^{-1}) and $Fe\mathbf{L^4}H_3$ (18.1 M^{-1} s^{-1}). The value of K_3'' (158 M^{-1}) is in agreement with the pK_a value (1.9) determined from static measurements at a 0.1 M ionic strength. The k_{-3}' value (635 s^{-1}) has no equivalent in the kinetic treatment to be related to the previously described micro-equilibrium. For $Fe\mathbf{L^2}H_3$ the value of k_4 (4440 M^{-1} s^{-1}) is consistent with the high lability of the catechol arm. For stage 3, we suggest that the pre-equilibrium [Equation (4)] is related to the Fe−N bond breaking of the 8-hydroxyquinoline arm leading to $Fe\mathbf{L^2}H_5$* (Figure 10) and that the last step [Equation (5)] is the change to the bidentate salicylate coordination of this arm ($Fe\mathbf{L^2}H_5$). The upper limit of 10 s^{-1} for k_3 is reasonable by comparison with the rate of rotation about the amide bond in hydroxamate ligands.[6]

Stage 4

In the last stage, leading from the tetradentate bis(salicylate) to the free ligand, at least two steps occur, corresponding to the Fe−O bond breakings of each salicylate arm. The rate constants for the leaving of the penultimate salicylate arms, k_2, could be measured only for $\mathbf{L^2}$ (33 s^{-1} M^{-1}) and $\mathbf{L^5}$ (4.9 s^{-1} M^{-1}). The smaller value for $Fe\mathbf{L^5}$ can be related to the bulkier access for the proton to the tetradentate complex with the pyridinophenol subunits in relation to the easy bond rotation between the pyridine and phenol moieties. The rate constants for the leaving of the last salicylate arm, k_1 (proton-dependent) and k'_1 (proton-independent) are well documented for all terms of the series (Table 2). About three orders of magnitude were observed, when measured, between k_2 and k_1 (or k'_1) for the release of two identical (salicylate) arms as already observed in related systems.[1]

Dependence of k_1 and k'_1 as a Function of Structure (Electrostatic Charge)

The important feature is that the rate constants k_1 and k_1' span over a range of several orders of magnitude: five orders for k_1 (184 to 0.0012×10^{-3} M^{-1} s^{-1}) and three and a half orders for k_1' (22 to 0.012×10^{-3} s^{-1}). Several trends in relation to the structure of the complex should be pointed out. The decrease of the rate constants k_1 and k_1' (except for $[Fe\mathbf{L^5}H_6]^{4+}$) in the series (Table 1) seems to be related mainly to the increase of the positive charges on the complexes evaluated without taking account of the sulfonate substituents, as in +3, +4, +5 and +6 for the iron(III) complexes with $\mathbf{L^3}$, $\mathbf{L^2}$, both $\mathbf{L^1}$ and $\mathbf{L^4}$ and $\mathbf{L^0}$, respectively. For the proton-dependent pathway (k_1) this is partly due to repulsion of the incoming H^+ by positive charges, suggesting that the dissociated 8-hydroxyquinoline arms of the ligand are maintained in proximity to the first coordination sphere of Fe^{III} probably through H-bonding between pyridinium nitrogen atoms and coordinated water molecules. It should be pointed out that k_1 for the complexes with the tris(8-hydroxyquinoline) ligands ($\mathbf{L^0}$ and $\mathbf{L^4}$) is 2 to 3 orders of magnitude slower than for the other complexes. This is probably due to enhanced repulsion for H^+ by positive charges suggesting a closer proximity for the dissociated arms than for the other ligands in $[Fe\mathbf{L^0}H_6]$ and $[Fe\mathbf{L^4}H_6]$. Indeed, pyridinium nitrogen atoms have been found to establish H-bonds with oxygen atoms coordinated to Fe^{III} in the structure of the tris(salicylate) complex with $\mathbf{L^0}$ forming a tight coordination sphere around the Fe^{III} center.[28] The value of 0.0079 M^{-1} s^{-1} for $[Fe\mathbf{L^5}H_6]^{4+}$ is high when compared with these highly charged complexes. This suggests a lower repulsion of the incoming H^+ by positive charges that are assumed to be far from the coordination sphere due to a free rotation of the pyridine ring relative to the phenol ring, thus disfavoring the formation of hydrogen bonds. For the proton-independent pathway, the decrease of k_1' parallels that of k_1.

Relationship between the Acid-Dependent and Acid-Independent Steps

The rate constants of these dissociations having acid-dependent and acid-independent steps vary in the same manner as a function of structure. We believe that this similarity is related to the structures of the transition states differing only by the presence of a proton. As the starting species is the same for these two steps, the transition state theory suggests a linear correlation between ln k_1 and ln k_1' [Equations (27) and (28)] as already discussed.[29,30]

$$\ln k_1 = \ln k_1' + \ln K_t \quad (27)$$

$$-\ln K_t = \Delta G_t^{\#}/RT \quad (28)$$

$\Delta G_t^{\#}$ is the free energy difference between the deprotonated and the protonated transition states, K_t may be considered as the protonation constant for the transition state and pK_{At} (= log k_1 − log k'_1) may be considered as a pseudo-pK_A of the transition state. A good correlation with a slope of 0.96 and an intercept $\ln K_t = 1.83$ ($pK_{At} = 0.80$) was obtained for the complexes with **L**[1], **L**[2], **L**[3] and **L**[5] (Figure 11). The correlation was not attempted for **L**[0] and **L**[4] since, for these ligands, k_1 values were only obtained as superior limits.

This correlation indicates that all the complexes follow the same dissociation mechanism from salicylate coordination. The protonation of the transition state is reasonably constant for this series. This implies that the hydroxy group is not implied in the transition state since its pK_a varies over a large range (5.6−9.23) in the free ligand. The Fe−O=C bond cleavage can therefore be suggested as the rate-limiting step for dissociation after a fast opening of the chelate ring as shown in Figure 12.

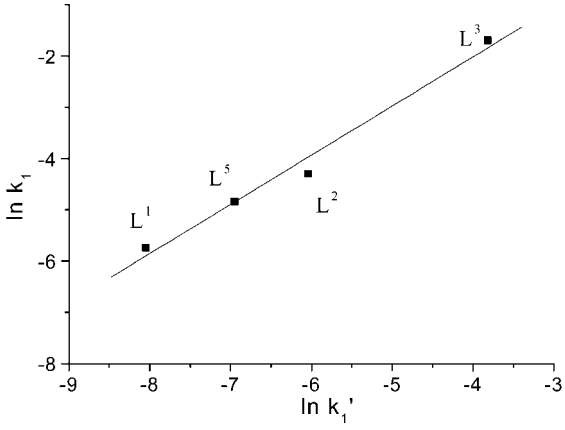

Figure 11. $\ln k_1$ vs. $\ln k_{-1}'$ for the final step dissociation of Fe**L**^{n} complexes; data were measured in aqueous 2.0 M $NaClO_4/HClO_4$ at 25 °C

Such a relationship has been observed for the dissociation of a large series of Fe^{III}-mono(hydroxamato) complexes yielding a slope of 0.9(1) in agreement with the theoretical value of 1, and an intercept $\ln K_1 = -0.6$ ($pK_{At} = -0.26$).[7] The correlation shows also that the transition state acidity of Fe^{III} (**L**[1] or **L**[2] or **L**[3] or **L**[5]) is lower than that of Fe^{III}(hydroxamic acid), i.e. that H^+ is more tightly bound in our series.

Linear Free Energy Relationships between k_1' and K_1'

The strong structural effect for the dissociation rate constants and the small dependence for the formation rate constants suggests a linear free energy relationships between $\ln k_1'$ and $\ln K_1'$ (K_1' has been calculated from k_1'/k_{-1}') [Equation (29)], where k_{-1}' (k_{-1}) is the formation rate constant when the active iron species is $FeOH^{2+}$ (Fe^{3+}). The theoretical basis for this correlation has been presented by Caudle and Crumbliss.[6]

$$\ln k_1' = \ln K_1' + \ln k_{-1}' \quad (29)$$

The plot $\ln k_1'$ vs. $\ln K_1'$ shown in Figure 13 (a) indicates a reasonably linear relation for the five complexes studied with a slope of 1.1 in agreement with the theoretical value of 1. This high degree of correlation suggests a similar mechanism in the final step of the dissociation. This implies a late transition state where the cleavage of the metal−ligand bonds are largely moved forward. The plot

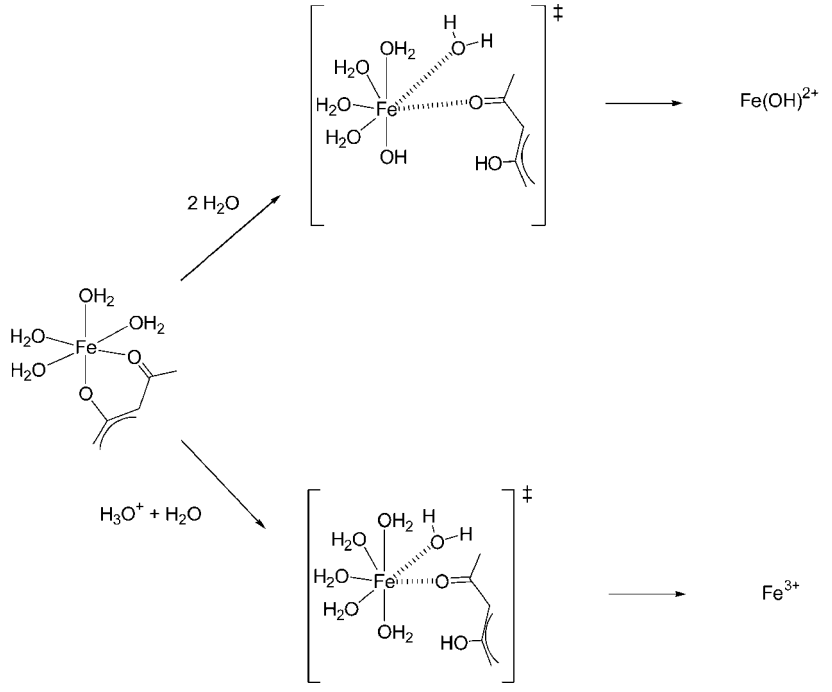

Figure 12. Transition states for proton-dependent and proton-independent dissociation of bidentate Fe−**L**^{n} complexes

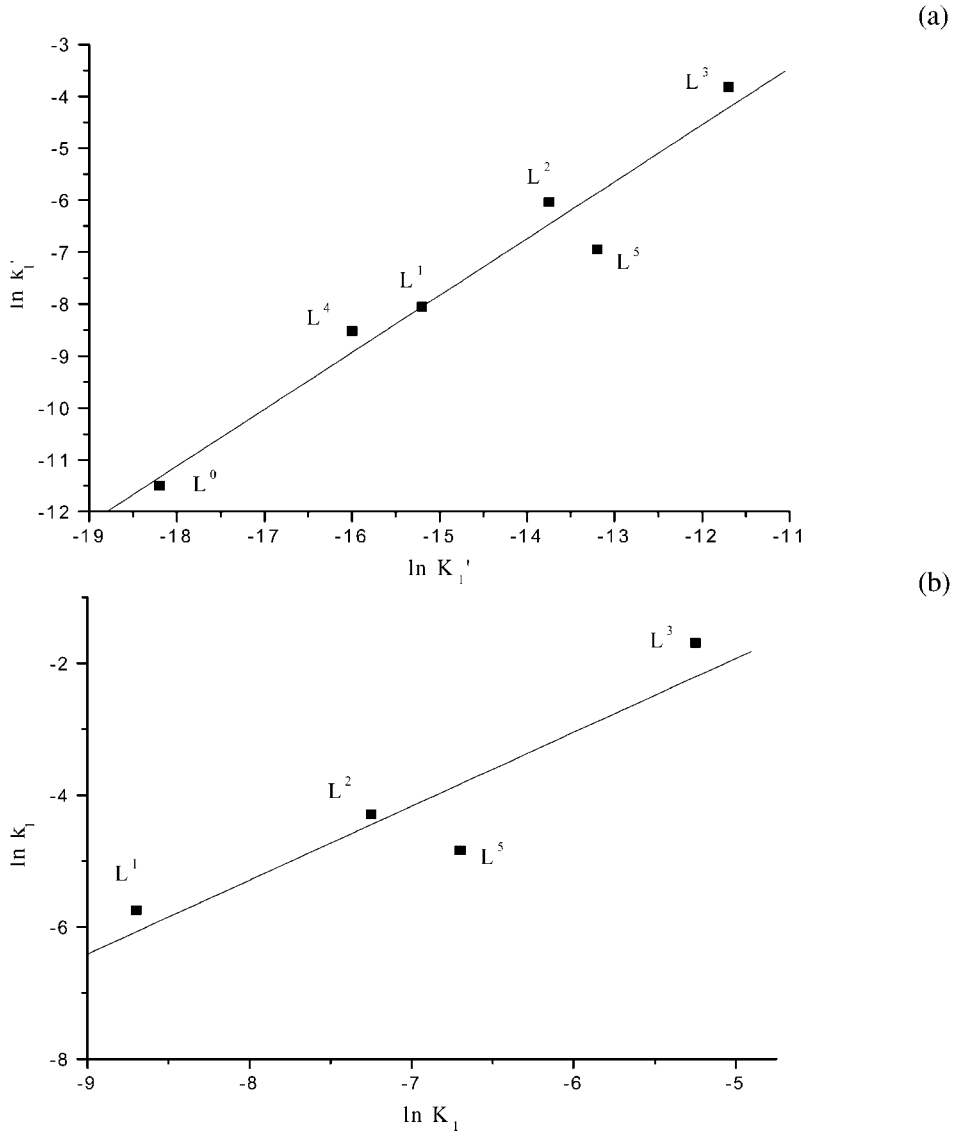

Figure 13. (a) ln k_1' vs. ln K_1' for proton-independent dissociation of bidentate Fe−**L**^{n} complexes; (b) ln k_1 vs. ln K_1 for proton-dependent dissociation of bidentate Fe−**L**^{n} complexes; data were measured in aqueous 2.0 M $NaClO_4/HClO_4$ at 25 °C

ln k_1 vs. ln K_1 (K'_1 calculated from K_1/K_{Fe}) also exhibits a reasonable correlation between data points for **L**^{1}, **L**^{2}, **L**^{3}, **L**^{5} with a slope of 1.1 (Figure 13, b) (a better correlation was obtained for the series **L**^{1}, **L**^{2}, **L**^{3}), as the correlation related to Equation (29) occurs. The proposed transition states are described in Figure 12.

Formation Kinetics

The rate-determining step is the coordination of Fe^{III} with one arm of the ligand through the salicylate coordination followed by a rapid coordination with a second arm of the ligand leading to the $[Fe\mathbf{L}H_5]^{n+}$ species. The spectra recorded during the formation of the complex using diode array device clearly show that coordination occurs through the 8-hydroxyquinoline arm for the mixed ligands **L**^{1} and **L**^{2}.

Ligand-substitution reactions at an iron center have been assumed to be controlled by water exchange from the inner coordination shell. The rate constants may be described according to the Eigen-Wilkins mechanism[31] with the fast formation step of an outer-sphere complex (K_{os}) followed by a rate-limiting step involving the water substitution of the monohydroxylated Fe^{III} species (k_{ex}) [Equation (30)], where S is a statistical factor to correct for the composition of the outer solvation shell.[6]

$$k_{-1}' = S\,K_{os}\,k_{ex} \tag{30}$$

The rate constant k_{-1}' was found to vary by a factor of about 5 for the six tripodal ligands studied. This result suggests charge effects of the ligand since increasing values for k_{-1}' were observed on going from $\mathbf{L^5}H_7^{4+}$, $\mathbf{L^0}H_7^{4+}$ to $\mathbf{L^1}H_7^{3+}$, $\mathbf{L^4}H_7^{3+}$, $\mathbf{L^2}H_7^{2+}$ and $\mathbf{L^3}H_7^{+}$ corresponding to a decreasing number of positive charges located on the N anchor and pyridine nitrogen atoms. The role of electro-

statics in charge effect concerning complexation reactions with hydroxamate ligands has been largely discussed by Crumbliss and al.[6,32] with discussion involving the Fuoss equation and the Debye-Hückel interionic potential involving a', the distance between the center of the positive charge of the metallic cation and the center of the charge (positive or negative) on the ligand.[33−36] (see Supporting Information, S19). The calculated K_{os} values are, from these considerations, 0.024 M^{-1} for **L^0** and **L^5** (+2, +4), 0.039 M^{-1} for **L^1** and **L^4** (+2, +3), 0.062 M^{-1} for **L^2** (+2, +2) and 0.100 M^{-1} for **L^3** (+2, +1) and were found to exhibit a good correlation with the k_{-1}' rate constants determined for ligands with an 8-hydroxyquinoline group (for $\mathbf{L^0}H_7^{4+}$, $\mathbf{L^1}H_7^{3+}$, $\mathbf{L^2}H_7^{2+}$, $k_{-1}' = 789$, 1320, 2240 M^{-1} s^{-1}, respectively) (Figure S20). This indicates that the complex formation follows the Eigen-Wilkins model. By taking a water exchange rate constant of 1.2×10^5 s^{-1} [37,38] in Equation (30), an S value of 2/7 can be deduced for $\mathbf{L^0}H_7^{4+}$, $\mathbf{L^1}H_7^{3+}$ and $\mathbf{L^2}H_7^{2+}$ which is a reasonable statistical correction for solvent shell composition for this series of ligands with similar structures.[1,32]

Some comments for the other terms of the series can be made. For $\mathbf{L^3}H_7^{+}$, complex data point of the correlation that k_{-1}'/K_{os} falls slightly below the line defined by the $\mathbf{L^0}H_7^{4+}$, $\mathbf{L^1}H_7^{3+}$ and $\mathbf{L^2}H_7^{2+}$ complexes suggesting that K_{os} has probably been overestimated. A lower a' value is reasonable owing to the smaller catechol ring size in comparison with an 8-hydroxyquinoline ring. For $\mathbf{L^4}H_7^{3+}$ (C anchor) the k_{-1}' rate constant (1750 M^{-1} s^{-1}) is intermediate between those for $\mathbf{L^1}H_7^{3+}$ and $\mathbf{L^2}H_7^{2+}$. This may be due to a larger bulkiness of $\mathbf{L^4}H_7^{3+}$ leading to a higher value for a' and hence a higher value for K_{os} in comparison with $\mathbf{L^1}H_7^{3+}$. The tripodal anchor contains one additional CH_2 and does not allow hydrogen bonding with the carbonyl oxygen atoms similar to ligands with a Tren anchor, thus increasing the bulkiness of $\mathbf{L^4}H_7^{3+}$ with respect to $\mathbf{L^1}H_7^{3+}$. For $\mathbf{L^5}H_7^{4+}$ the k_{-1}' rate constant (514 M^{-1} s^{-1}) is lower than that for $\mathbf{L^0}H_7^{4+}$ (789 M^{-1} s^{-1}). A possible explanation could be that the entry of this ligand in the second coordination sphere of Fe^{III} is less favored owing to the flexibility of the binding cavity that allows rotation of the pyridine ring relative to the phenol ring and leads consequently to a smaller S value.

Conclusion

This work is the first report on the acid dissociation (and formation) kinetics of iron(III) complexes with a series of tripodal ligands, four homopodates [with two types of anchor (*tren* or C-anchor)], three types of arm (catechol or 8-hydroxyquinoline or pyridinophenol) and two heteropodates (mixing catechol or 8-hydroxyquinoline).

Analysis of kinetic data shows that there is a common mechanism in all the series when the ligand structure is varied. The mechanism of the dissociation is more complex than the successive departure of the three arms around the iron(III) as observed in the literature for linear ligands[1] (three successive bidentate moieties). The dissociation of the first arm (from a hexadentate to a tetradentate complex) is in all cases observed but too fast to be measured. The dissociation then follows a process going from the tetradentate complex with the originally di-coordination of the two concerned arms to the tetradentate bis(salicylate) complex. During this process, bond cleavage of Fe−N_{pyr} or Fe−O with protonation of N or O, followed by proton-independent Fe−O(=C) bond formation to close the salicylate ring could be characterized in most cases. The comparison of these reaction rate constants reflects the influence of chelate donor strength (catechol or pyridinophenol vs. 8-hydroxyquinoline) and the rate of rotation of the amide bond between the anchor and the arm in question. The rate constants for the leaving of the ultimate salicylate arm indicate a proton-dependent (k_1) and a proton-independent (k'_1) reaction. The rate constants k_1 and k_1' span over a range of several order of magnitude: five orders for k_1 (184 to 0.0012 $\times 10^{-3}$ M^{-1} s^{-1}) and three and a half orders for k'_1 (22 to 0.012 $\times 10^{-3}$ s^{-1}). The role of electrostatics in control of the dissociation rate of the last step is evidenced for the 8-hydroxyquinoline moieties. Interesting correlations could be obtained which yielded information on the transition states for the two mechanisms.

From thermodynamic and kinetic studies on aqueous solutions of such Fe^{III} complexes, we believe that analysis of rates of Fe−N or Fe−O bond cleavage of the species and the proposed structures for the transition states will help in the designing of new ligands for appropriate exchange of Fe^{III} in biological systems.

Experimental Section

Materials: All commercial reagents were of the highest purity grade and were used without further purification. Iron(III) stock solutions were prepared by dissolving the appropriate amount of ferric perchlorate hydrate (Aldrich) in standardized $HClO_4$ solution. The solutions were standardized for ferric ion concentration spectrophotometrically by using a molar extinction coefficient of 4160 M^{-1}·cm^{-1} at 240 nm.[39] The ligands were synthesized according to procedures previously described (**L^0**,[17a] **L^1**,[20] **L^2**,[20] **L^3**,[15] **L^4**,[40] **L^5**[18]).

Kinetics Studies: Kinetic measurements were performed with a KINSPEC UV (BIO-LOGIC Company, Claix, France) stopped-flow spectrophotometer equipped with a diode array detector (J & M) and connected to a microcomputer. The reported rate constants are the average of about 6 repeat determinations (standard deviation in the range 1−2%). The kinetic data were treated on-line with the commercial BIO-KINE program (BIO-LOGIC Company, Claix, France). The ionic strength was fixed at $I = 2$ M ($NaClO_4$, $HClO_4$) due to the H^+ concentrations which were up to 1 M. This allowed comparisons with literature data. Formation kinetics were carried out under pseudo-first-order conditions at 25 °C with Fe^{III} in excess with respect to the ligand. The Fe^{III} concentration spanned the range 5×10^{-3} to 3×10^{-3} M for each H^+ concentration which was over the range 0.03 to 0.1 M. A solution containing Fe^{III} and H^+ and a solution containing the ligand (1×10^{-4} M) at the same ionic strength were mixed on the stopped-flow apparatus. In each case, first order kinetics were observed. The acid

hydrolysis kinetics of the $Fe^{III}-\mathbf{L}^{n}$ complexes were studied under pseudo-first-order conditions in the presence an of excess protons ($[H^+]$ range 0.01 to 1 M) at 25 °C. The initial pH of the $Fe^{III}-\mathbf{L}^{n}$ solution (ca. 1×10^{-4} M) was ca. 5.

Acknowledgments

The authors thank Professor J.-L. Pierre (LEDSS) for his interest in these studies and Professor P. Baret for managing the syntheses of the ligands $\mathbf{L}^{n}$.

[1] A.-M. Albrecht-Gary, A. L. Crumbliss, *Met. Ions Biol. Syst.* **1998**, *35*, 243−327.
[2] B. F. Matzanke, G. Müller-Matzanke and K. N. Raymond in *Physical Bioinorganic Chemistry Series: Iron Carriers and Iron Proteins* (Ed.: T. M. Loehr), VCH, New York, **1989**, p.1.
[3] J. R. Telford, K. N. Raymond in *Comprehensive Supramolecular Chemistry* (Eds.: J. M. Lehn, G. W. Gokel), Pergamon Press, London, **1996**, p. 245.
[4] R. R. Crichton in *Inorganic Biochemistry of Iron Metabolism*, John Wiley & Sons, Chichester, **2001**.
[5] [5a] J.-F. Briat, S. Lobréaux in *Metals Ions in Biological Systems* (Eds.: A. Sigel, H. Sigel), Marcel Dekker, Inc., New York, **1998**, vol. 35, chapter 14, p. 563; [5b] R. R. Crichton, R. J. Ward, chapter 16, p. 633; [5c] G. S. Tilbrook, R. C. Hider, chapter 18, p. 691.
[6] M. T. Caudle, A. L. Crumbliss, *Inorg. Chem.* **1994**, *33*, 4077−4085.
[7] M. T. Caudle, L. P. Cogswell, A. L. Crumbliss, *Inorg. Chem.* **1994**, *33*, 4759−4773.
[8] B. Monzyk, A. L. Crumbliss, *J. Am. Chem. Soc.* **1982**, *104*, 4921−4929.
[9] M. Birus, Z. Bradic, G. Krznaric, N. Kujundzic, M. Pribanic, P. C. Wilkins, R. G. Wilkins, *Inorg. Chem.* **1987**, *26*, 1000−1005.
[10] H. Boukhalfa, A. L. Crumbliss, *Inorg. Chem.* **2000**, *39*, 4318−4331.
[11] H. Boukhalfa, T. J. Brickman, S. K. Armstrong, A. L. Crumbliss, *Inorg. Chem.* **2000**, *39*, 5591−5602.
[12] Y. Hara, L. Shen, A. Tsubouchi, M. Akiyama, *Inorg. Chem.* **2000**, *39*, 5074−5082.
[13] Y. Hara, M. Akiyama, *J. Am. Chem. Soc.* **2001**, *39*, 7247−7256.
[14] S. J. Rodgers, C. W. Lee, C. Y. Ng, K. N. Raymond, *Inorg. Chem.* **1987**, *26*, 1622−1625.
[15] F. Thomas, C. Béguin, J.-L. Pierre, G. Serratrice, *Inorg. Chim. Acta* **1999**, *291*, 148−157.
[16] C. Y. Ng, S. J. Rodgers, K. N. Raymond, *Inorg. Chem.* **1989**, *28*, 2062−2066.
[17] [17a] P. Baret, C. Béguin, H. Boukhalfa, C. Caris, J.-P. Laulhère, J.-L. Pierre, G. Serratrice, *J. Am. Chem. Soc.* **1995**, *117*, 9760−9761. [17b] G. Serratrice, H. Boukhalfa, C. Béguin, P. Baret, C. Caris, J.-L. Pierre, *Inorg. Chem.* **1997**, *36*, 3898−3910.
[18] P. Baret, C. Béguin, G. Gellon, J.-L. Pierre, G. Serratrice, F. Thomas, J.-P. Laulhère, E. Saint-Aman, *Eur. J. Inorg. Chem.* **2000**, 1219−1227.
[19] M. Meyer, J. R. Telford, S. M. Cohen, D. J. White, J. Xu, K. N. Raymond, *J. Am. Chem. Soc.* **1997**, *119*, 10093−10103; S. M. Cohen, B. O'Sullivan, K. N. Raymond, *Inorg Chem.* **2000**, *96*, 4339−4346.
[20] A.-M. Albrecht, S. Blanc, F. Biaso, F. Thomas, P. Baret, G. Gellon, J.-L. Pierre, G. Serratrice, *Eur. J. Inorg. Chem.* **2003**, 2596−2605.
[21] F. Biaso, Thesis, Université Joseph Fourier, Grenoble, **2002**.
[22] D. Imbert, P. Baret, D. Gaude, I. Gautier-Luneau, G. Gellon, F. Thomas, G. Serratrice, J.-L. Pierre, *Chem. Eur. J.* **2002**, *8*, 1091−1100.
[23] D. Imbert, F. Thomas, P. Baret, G. Serratrice, D. Gaude, J.-L. Pierre, J.-P. Laulhère, *New J. Chem.* **2000**, *24*, 281−288.
[24] C.-W. Lee, D. J. Ecker, K. N. Raymond, *J. Am. Chem. Soc.* **1985**, *107*, 6920−6923.
[25] R. M. Milburn, W. C. Vosburgh, *J. Am. Chem. Soc.* **1955**, *77*, 1352−1355.
[26] A. Shanzer, S. Libman, S. Lifson, *Pure Appl. Chem.* **1992**, *64*, 1421−1428.
[27] D. Chapon, G. Serratrice, unpublished results.
[28] G. Serratrice, P. Baret, H. Boukhalfa, I. Gautier-Luneau, D. Luneau, J.-L. Pierre, *Inorg. Chem.* **1999**, *38*, 840−841.
[29] A. L. Crumbliss, in *CRC Handbook of Microbial Iron Chelates* (Ed.: G. Winkelman), CRC Press, Boca Raton, Fl, **1991**, chapter 7.
[30] L. E. Asher, E. Deutsch, *Inorg. Chem.* **1973**, *12*, 1774−1778.
[31] M. Eigen, R. G Wilkins, "Mechanism of Inorganic Reactions", *Adv. Chem. Ser.* **1965**, *55*.
[32] J. I. Wirgau, I. Spasojevic, H. Boukhalfa, I. Batinic-Haberle, A. C. Crumbliss, *Inorg. Chem.* **2002**, *41*, 1464−1473.
[33] R. M. Fuoss, *J. Am. Chem. Soc.* **1958**, *80*, 5059−5061.
[34] M. Z. Eigen, *Phys. Chem.* **1954**, *1*, 176−185.
[35] C.-T. Lin, D. B. Rorabacher, *Inorg. Chem.* **1973**, *12*, 2402−2410.
[36] N. J. Hair, J. K. Beattie, *Inorg. Chem.* **1977**, *16*, 245−250.
[37] M. Grant, R. B. Jordan, *Inorg. Chem.* **1981**, *20*, 55−60.
[38] T. W. Swaddle, A. E. Merbach, *Inorg. Chem.* **1981**, *20*, 4212−4216.
[39] R. Bastian, R. Weberling, F. Palilla, *Anal. Chem.* **1956**, *28*, 459−462.
[40] D. Imbert, Thesis, Université Joseph Fourier, Grenoble, **2000**.

Received June 25, 2004
Early View Article
Published Online March 5, 2004

